Numerical study on unfavorable influences of methane hydrate production on dynamic behavior of seabed sediments during an earthquake

Etude numérique sur l'influence défavorable de la production de méthane hydrate sur le comportement dynamique des sédiments de fond marin pendant un séisme

Toshifumi Akaki, Sayuri Kimoto
Civil and Earth Resources Engineering, Kyoto University, Japan, akaki.toshifumi.33w@st.kyoto-u.ac.jp

ABSTRACT: Oceanic methane hydrates generally exist in relatively shallow and uncemented seabed ground layers. Moreover, since they are often found in seismically active regions, including the Nankai Trough area of Japan, there is a risk of large earthquakes during methane hydrate production. Seabed sediments damaged by the methane hydrate production may show unfavorable seismic behaviors, and it may result in seabed slides. In the present study, numerical analyses have been performed for two different models to investigate the effects of gas production on the dynamic behavior of seabed sediments during earthquake. One model is with clay layers except methane hydrate-bearing layer and the other includes a sand layer between clay layers 40m bellow seafloor. From the simulation results, the maximum velocity during earthquakes increased with increasing gas production period for some cases. The increase of the maximum velocity is induced by reduction of the mean skeleton stress in clay layers during gas production. The result indicates that dynamic behaviors of seabed sediments during earthquake are possible to be influenced by gas production.

RÉSUMÉ: Les hydrates de méthane océanique existent généralement dans les couches de sol des fonds marins peu profondes et non cimentées. Aussi, vu qu'ils sont souvent trouvés dans les régions sismiquement actives, y compris le bas fond de Nankai du Japon, il y a un risque de grands séismes lors de leur production. Les sédiments des fonds marins endommagés par la production d'hydrate de méthane peuvent montrer des comportements sismiques défavorables, pouvant résulter à des glissements de fonds marins. Les analyses numériques ont été réalisées sur deux modèles différents pour étudier l'influence de la production de gaz sur les comportements dynamiques de ces sédiments lors des séismes. L'un avec des couches d'argile, à l'exception du méthane hydrate en couche supérieur et l'autre avec une couche de sable entre les couches d'argile à 40m en fond de mer. Ces simulations montrent que la vitesse maximale lors des séismes croît avec une croissance du temps de production de gaz pour certains cas. L'augmentation de cette vitesse est induite par une réduction du « skeleton stress » moyen dans les couches d'argile lors de la production de gaz. Le résultat indique que les comportements dynamiques des sédiments durant les séismes peuvent être influencés par la production de gaz.

KEYWORDS: methane hydrate, earthquake, depressurization

1 INTRODUCTION

Nowadays, Methane hydrates which is solid crystalline compounds consist of methane and water are viewed as a new energy resource, since large amounts of methane gas can be extracted from the methane hydrates. They are naturally found in permafrost sediments and in deep seabed grounds under high pressure and low temperature conditions.

Since methane hydrates are solid substances, they must be dissociated into methane gas and water in the ground layer. As oceanic methane hydrates generally exist in relatively shallow and uncemented seabed ground layers, large deformation of seabed sediments may occur due to methane hydrate dissociation and external force for gas production such as heating and depressurization. Since oceanic methane hydrates are often found in seismically active regions, including the Nankai Trough area of Japan, there is a risk of large earthquakes during the period of gas production. Nankai Trough is where the world's first offshore production test of methane hydrates was conducted for methane hydrate concentration zones and is also in fault region of Nankai earthquake (Figure. 1). The sediment deformation and degradation of the soil structure is induced by the gas production. If large earthquakes occur during gas production, seabed sediments damaged by the gas production may show unfavorable seismic behaviors, and may become a trigger of seabed slides.

In the present study, we have used a numerical method which can simulate the seismic behaviors of seabed grounds and chemo-thermo-mechanically coupled behaviors during gas production, such as phase changes from hydrates to water and gas, temperature changes, ground deformation and the flow of pore fluids. Numerical analyses were performed for two models to investigate effects of gas production on dynamic behavior of seabed sediments during earthquake.

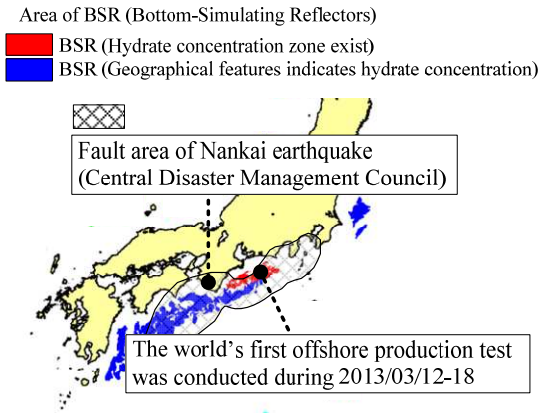

Figure 1. The world's first offshore production test site, methane hydrate concentration zones around japan and fault area of Nankai earthquake (MH 21, http://www.mh21japan.gr.jp/).

2 NUMERICAL METHOD

2 .1 *General setting*

We use continuum approach for modelling of hydrate-bearing sediments. The sediments are composed of four phases, namely, soil particles (S), hydrates (H), water (W) and methane gas (G) (Figure 2). For simplicity, we assume that the soil particles and the hydrates move together.

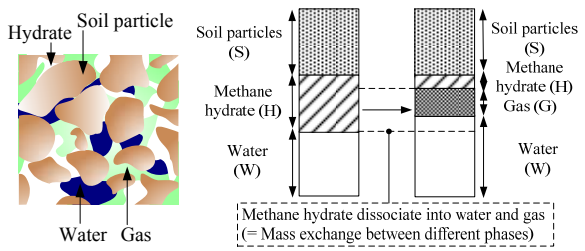

Figure 2. Definition of phases of hydrate-bearing soil.

Volume fraction n^α is defined as the local ratio of the volume element with respect to the total volume, as follows:

$$n^\alpha = V^\alpha / V, \quad \sum_\alpha n^\alpha = 1 \quad (\alpha : S, H, W, G) \tag{1}$$

The volume fraction of the voids n, the volume fraction of fluid n^F, the saturation s_r and the hydrate saturation s_r^H are given by

$$n = 1 - n^S, \quad n^F = n - n^H, \; s_r = n^W / n^F, \quad s_r^H = n^H / n \tag{2}$$

2 .2 *Material derivatives*

The material derivative following each phase is defined as:

$$\frac{d^\alpha(\,)}{dt} = \frac{\partial(\,)}{\partial t} + \boldsymbol{v}^\alpha \cdot \nabla(\,) \quad (\alpha : S, H, W, G) \tag{3}$$

where $\boldsymbol{v}^\alpha$ is the velocity vector for each phase. The material time derivative following the soil particle phase equals the one following the hydrate phase from the assumption, $\boldsymbol{v}^S = \boldsymbol{v}^H$, and the material time derivative following the solid phase (SH) can be defined as:

$$\dot{(\,)} = \frac{d(\,)}{dt} \equiv \frac{d^{SH}(\,)}{dt} = \frac{d^S(\,)}{dt} = \frac{d^H(\,)}{dt} \tag{4}$$

2 .3 *Stress variable*

We use the skeleton stress $\boldsymbol{\sigma}'$ given by following equation as the basic stress variable for the solid phase.

$$\boldsymbol{\sigma}' = \boldsymbol{\sigma} + P^F \boldsymbol{I}, \quad P^F = s_r P^W + (1 - s_r) P^G \tag{5}$$

where $\boldsymbol{\sigma}$ is the total stress tensor, P^W and P^G is the water and gas pressure, P^F is the average pore pressure.

2 .4 *Conservation laws*

Following equations can be derived from conservation laws for each phase. the conservation of momentum for mixture (eq.(6)), The conservation of mass for soil particles and hydrates (eq.(7)), the continuity equations for water and gas (eq.(8) and (9)) and the conservation of energy for mixture (eq.(10) and eq.(11)) are used for calculations.

$$\rho \dot{\boldsymbol{v}}^{SH} = \nabla \cdot \boldsymbol{\sigma}^T + \rho \boldsymbol{b} \tag{6}$$

$$\dot{n}^S + n^S \nabla \cdot \boldsymbol{v}^{SH} = 0, \quad \dot{n}^H + n^H \nabla \cdot \boldsymbol{v}^{SH} = \frac{\dot{m}^H}{\rho^H} \tag{7}$$

$$s_r \nabla \cdot \boldsymbol{v}^{SH} + \dot{s}_r n^F + \nabla \cdot \boldsymbol{V}^W = s_r \frac{\dot{m}^H}{\rho^H} + \frac{\dot{m}^W}{\rho^W} \tag{8}$$

$$(1 - s_r) \nabla \cdot \boldsymbol{v}^{SH} - \dot{s}_r n^F + \nabla \cdot \boldsymbol{V}^G + (1 - s_r) n^F \frac{\dot{\rho}^G}{\rho^G} = (1 - s_r) \frac{\dot{m}^H}{\rho^H} + \frac{\dot{m}^G}{\rho^G} \tag{9}$$

$$(\rho c)^M \dot{\theta} + \left(\rho^W c^W \boldsymbol{V}^W + \rho^G c^G \boldsymbol{V}^G\right) \cdot \nabla \theta = \boldsymbol{\sigma}'^T : \boldsymbol{D}^{vp} + \nabla \cdot \left(\lambda^M \nabla \theta\right) + \dot{Q}^H_{diss} \tag{10}$$

$$(\rho c)^M = \sum_\alpha n^\alpha \rho^\alpha c^\alpha, \; \lambda^M = \sum_\alpha n^\alpha \lambda^\alpha \quad (\alpha = S, H, W, G) \tag{11}$$

where θ is the temperature, $\boldsymbol{V}^W$ and $\boldsymbol{V}^G$ are water and gas average relative velocity to solid phase, ρ^W, ρ^G and ρ^H are density for water, gas and hydrate, ρ is density for mixture, $\dot{m}^W$, $\dot{m}^G$ and $\dot{m}^H$ are the water, gas and hydrate mass-generation rate per unit, c^α and λ^α are the specific heat and the coefficients of thermal conductivity for each phase, respectively. $\boldsymbol{V}^W$ and $\boldsymbol{V}^G$ are given by Darcy type equations. $\boldsymbol{D}^{vp}$ is the viscoplastic stretching tensor, $\dot{Q}^H_{diss}$ is heat generation rate per unit volume induced by hydrate dissociation.

2 .5 *Constitutive equations*

We used a cyclic elasto-viscoplastic model based on overstress type viscoplastic theory with the nonlinear kinematic hardening rules, the structural degradation for solid phase and hydrate saturation dependency of the stress-strain behaviors (Akaki et al., 2016). The elastic behavior is given by a generalized Hooke type of law. The shear modulus, which is important for seismic response analysis, decrease with accumulation of viscoplastic shear strain and the hydrate saturation. We assumed the ideal gas for the gas phase and van Genuchten model is used for soil-water characteristic curve. Kim-Bishnoi equation (Kim and Bishnoi, 1987) is used for methane hydrate dissociation rate which determine the mass generation rates per unit volume, $\dot{m}^W$, $\dot{m}^G$ and $\dot{m}^H$.

3 CALCULATION CONDITIONS

Numerical analyses were performed for two different models to investigate the effects of gas production by depressurization on the dynamic behaviors of seabed sediments during earthquake. The finite element mesh and the boundary conditions used in the simulations are shown in Figure 3. A horizontally layered ground under two-dimensional plane strain conditions is assumed. The sediment is divided into 6 layers and the layer L3 in Figure 3 is a methane hydrate-bearing layer. The hydrate-bearing layer, with a thickness of 60 m, is 100 m bellow the seabed. In the present study, we have conducted calculations with two different models. For Case 1, layers L1, L2, L3, L4 and L6 are basically same material except elastic shear modulus, and their material parameters are determined from undrained triaxial tests and constant rate of strain rate consolidation test conducted for low liquidity clay samples recovered from the area of the first Japanese offshore production test at the Eastern Nankai Trough (Nishio et al. 2013). Simulation results of the undrained triaxial compression tests are shown in Figure 4. For Case 2, there is a sand layer in layer L2 at a depth 40 m-70 m below the seafloor as shown in Figure 3. Material parameters for the sand layer is determined from a drained triaxial compression test for Toyoura sand under 1MPa initial mean effective stress conducted by Hyodo et al (2013). Simulation results of the drained triaxial compression tests are shown in Figure 5. Clay shows compressive behavior at first and then exhibits dilative behavior under triaxial shear. On the other hand, Toyoura sand shows dilative behavior during shear loading. The methane hydrates are dissociated by depressurization. Material parameters for the clay and the methane hydrate-bearing layer are correspond with layer L4 and L5 in a former study respectively (Akaki et al. 2016). The depressurization source is placed at the bottom side of the methane hydrate-bearing layer. The pore water pressure and the pore gas pressure at the depressurization source are depressurized from 7.0 MPa to 3.5 MPa during a period of

about 14 hours, as shown in Figure 6. A gas production process was firstly simulated, and then a dynamic analyses for the earthquake process was conducted. The gas production periods before earthquake are assumed to be 0day, 9days, 25days and 140days. A input ground motion is illustrated in Figure 7, which is an expected earthquake motion at the site where the first methane hydrate production test was conducted (Figure 1) using the EMPR by Sugito et al. (2000). The magnitude of the hypothetical earthquake is 9.0 and the epicenter is off the coast of the Kii Peninsula.

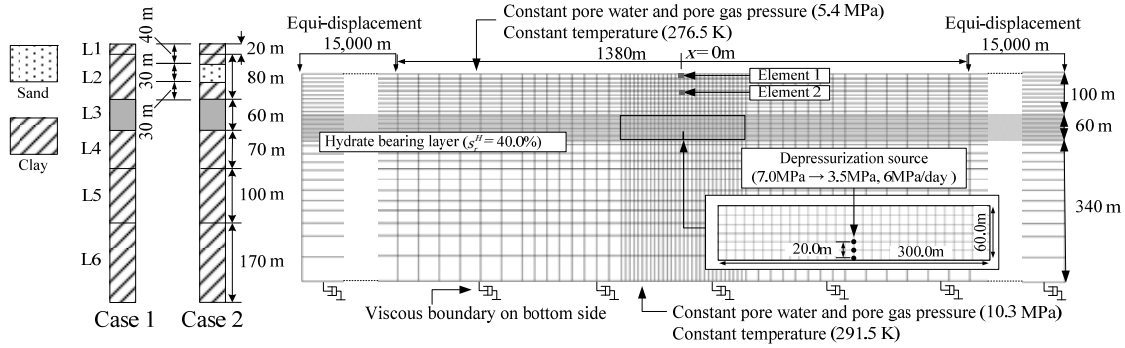

Figure 3. Finite element mesh and boundary conditions.

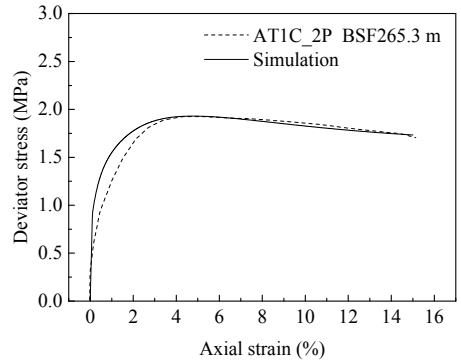

(a) Axial strain – deviator stress relations

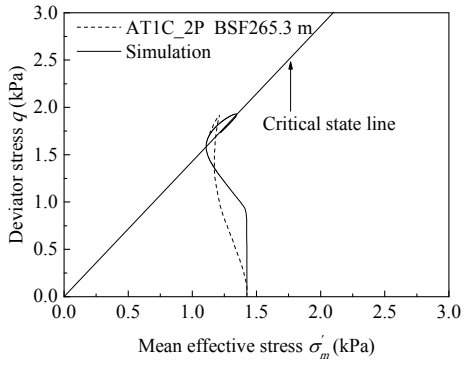

(b) Effective stress paths

Figure 4. Simulation results of undrained triaxial tests for the clay material.

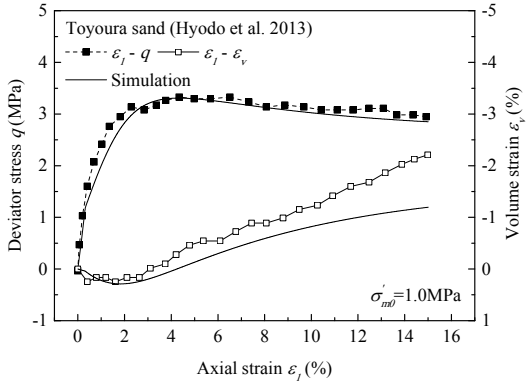

Figure 5. Simulation results of drained triaxial test for the sand material.

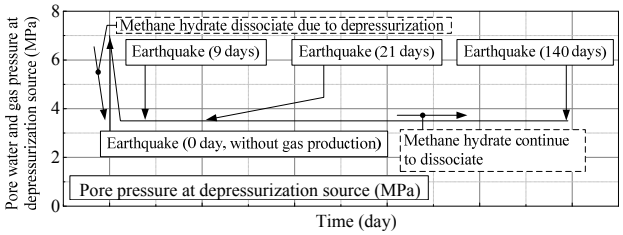

Figure 6. Time profile of pressure at production well.

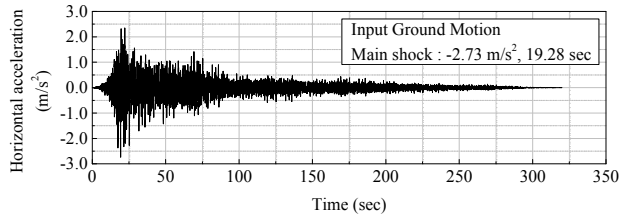

Figure 7. Input ground motion

4 SIMULATION RESULTS

Distributions of the vertical strain after 140 days gas production for Case 1 and Case 2 are shown in Figure 8. Extensional vertical deformation occurs during gas production from seafloor to upper boundary of methane hydrate-bearing layer. The negative vertical strain (tension strain) for Case 1 is larger than Case 2. Thus the sediments experience extension shear during gas production. Non-dimensional effective stress paths during gas production for elements 1 and 2 shown in Figure 3 for Case 1 and Case 2 are displayed in Figure 9. A horizontal axis is a ratio between the mean skeleton stress and the initial value. A vertical axis is the stress ratio between the second invariant of the deviatoric stress tensor and the mean skeleton stress. Effective stress reduction is found on elements 1 and 2 for clay (Case 1), oppositely effective stress increases during gas production for sand (Case 2). This reduction of the mean skeleton stress would be likely for soils which show compressive behavior during shear loading. Decrease of the mean skeleton stress of a soil results in the reduction of the stiffness. Element 1 with clay shows almost same effective stress paths for both cases, that is, sand layer for Case 2 have a few effect on stress paths of surrounding clay layers during gas production.

Figure 10 shows distributions of maximum velocity during earthquake in depth on the center of seafloor (x = 0 shown in

Figure 3). The distributions for different gas production periods (0day, 9days, 25days and 140days) are displayed. For Case 1, the maximum velocities which is related to shear strain in sediments during earthquake increases with increasing gas production period before earthquake. This is because the mean skeleton stress of seabed sediments shown in Figure 9 decreases during gas production and reduction of stiffness of the seabed sediments occur, and the degree of the reduction of stiffness becomes large with increasing gas production period. For Case 2, increase of maximum velocities during earthquake is seen, but it is considerably smaller than Case 1. Mean skeleton stress increase in sand layer between clay layers results in increase of stiffness, and that reduce the increase of the maximum velocities. From these results, it is found that oscillation and shear strain of sediments during earthquake are possible to become large due to the decrease of the mean skeleton stress during gas production depending on material properties.

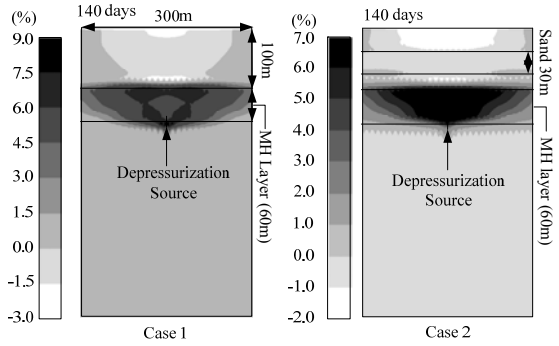

Figure 8. Distribution of vertical strain after 140 days gas production.

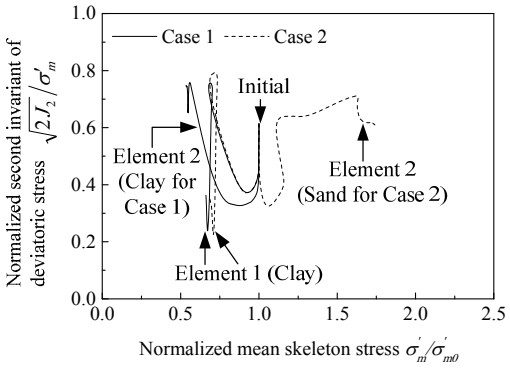

Figure 9. Non-dimensional effective stress paths for element 1 and 2.

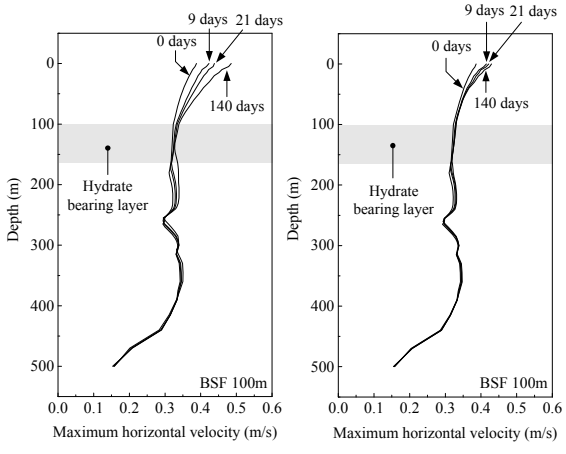

Figure 10. Distribution of maximum velocity during earthquake in depth on the center of seafloor (x=0m).

5 CONCLUSIONS

In the present study, we have used a numerical method which can simulate the seismic behaviors of seabed grounds including chemo-thermo-mechanical coupled behaviors during gas production from methane hydrate-bearing sediments. Numerical analyses were performed under two-dimensional plane strain conditions for the seabed sediments with methane hydrate-bearing layer to investigate effects of gas production on dynamic behavior of seabed sediments during earthquake. The analyses were conducted for two models. One model is with clay layers except methane hydrate-bearing layer and the other is with a sand layer between clay layers above the methane hydrate-bearing layer. From the results, following conclusions were obtained.

1. Extensional vertical deformation during gas production was found in sediments from seafloor to top of methane hydrate-bearing layer.
2. Mean skeleton stress reduction from seafloor to 50m in depth occurs during gas production depending on material properties of soils. This reduction would be likely to occur for soils which show compressive behavior during shear loading.
3. Maximum velocity which is related to shear strain during earthquake increases with increasing gas production period. The stiffness of clay layers near seafloor decreases due to the mean skeleton stress reduction during gas production and it would result in the increase of the maximum velocity during earthquake.

Above conclusions indicate that the dynamic behavior of seabed sediments during earthquake are possible to be influenced by gas production depending on material properties of the seabed grounds, though it should be taken into account that calculations in this study have been conducted under two-dimensional plane strain conditions, and it would lead to somewhat large evaluation of deformation during gas production.

6 REFERENCES

Akaki T., Kimoto S. and Oka F. 2016. Chemo-thermo-mechanically coupled seismic analysis of methane hydrate-bearing sediments during a predicted Nankai Trough Earthquake. Int. J. Numer. Anal. Meth. Geomech., 4, 2207-2237.

Kim H.C., Bishnoi P.R., Heidemann R.A. and Rizvi S.S.H. 1987. Kinetics of methane hydrate decomposition. Chemical Engineering Science, 42 (7), 1645-1653.

Nishio S., Ogisako E., Denda A., Hirakawa H., Tanaka H., Hyodo M. and Mitachi T. 2013. Geotechnical Properties of Sediment Core Samples Recovered from Eastern Nankai Trough. In Proceedings of the 13th Japan Symposium on Rock Mechanics, Japan, January. 377-382. (in Japanese)

Hyodo M., Yoneda J., Yoshimoto N. and Nakata, Y. 2013. Mechanical and dissociation properties of methane hydrate-bearing sand in deep seabed. Soils and Foundations, 53(2), 299-314.

Akaki T., Kimoto S. and Oka F. 2016. Chemo-thermo-mechanically coupled seismic analysis of methane hydrate-bearing sediments during a predicted Nankai Trough Earthquake. International Journal for Numerical and Analytical Methods in Geomechanics. 40, 2207–2237.

Sugito M., Furumoto Y., and Sugiyama T. 2000. Strong Motion Prediction on Rock Surface by Superposed Evolutionary Spectra, 12th World Conference on Earthquake Engineering, CD-ROM, Auckland, New Zealand, January.